Special Papers

SSAM: Solid-State Automated Microscope

IAN T. YOUNG, BALASUBRAMANIAN, DOUGLAS L. DUNBAR, RICARDO L. PEVERINI, AND ROBERT P. BISHOP, MEMBER, IEEE

Abstract—**A new microscope system that is designed to provide images for a computer has been built and tested. This system differs from previous computerized microscopes in that the fundamental design parameters have been tuned to the computer as the receiver of the image instead of the human visual system. This solid-state automated microscope system (SSAM) simultaneously provides wide-field (2 mm), high-resolution (0.5 μ), high signal-to-noise images (>53 dB) at data rates of 5×10^6 pixels/s. Various methods have been developed and used to test the design specifications of the system against the actual performance.**

I. Historical Background

MAN'S first microscope was almost certainly a drop of water. Acting as a hemispherical lens on the surface of a leaf or the back of a hand, it provided magnification on the order of 1.3×. As early as the end of the 16th century Hans and Zaccharis Janssen of Middelburg, The Netherlands constructed the first compound (multiple lens) microscope. While Galileo is considered to be the first scientific user of a microscope [1], it was the work of van Leeuwenhoek in Leiden, Hooke in London, and Malpighi in Italy that demonstrated the usefulness and, indeed, necessity of the microscope for biological and medical studies. Van Leeuwenhoek, with an appointment as a custodian in the City Hall of Delft, used his spare time to construct over 500 simple (one-lens) microscopes. The lenses of these microscopes were exquisitely made and provided magnifications up to 200×. With these microscopes, first devised to examine drapery fabrics, van Leeuwenhoek described protozoa, bacteria, and human sperm [2]-[4]. Thus, the use of the microscope as a high-technology scientific instrument goes back at least 350 years.

Manuscript received February 13, 1981; revised. This work was supported by the National Cancer Institute under Grant CA-28833 and the U.S. Department of Energy under Contract W-7405-ENG-48.

I. T. Young is with the Department of Applied Physics, Technical University Delft, Delft, The Netherlands.

Balasubramanian is with Digital Optics, Inc., Sunnyvale, CA 94086.

D. L. Dunbar is with the Department of Electrical Engineering, Los Alamos National Laboratory, University of California, Los Alamos, NM 87545.

R. L. Peverini is with the School of Medicine, Loma Linda University, Loma Linda, CA 92354.

R. P. Bishop is with Beltronics, Inc., Brookline, MA 02146.

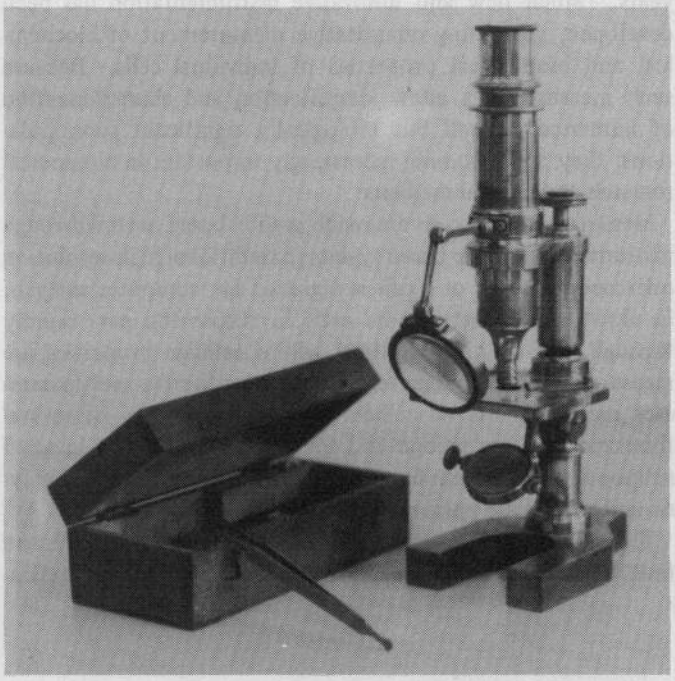

Fig. 1. Compound monocular microscope manufactured in Paris by E. Hartmack Co., circa 1880. Notice that the basic form and size of this instrument is the same as that used in today's laboratory microscopes (from a collection in The Netherlands).

The design of the microscope continued to evolve and by the middle of the 19th century it had assumed a form similar to what is seen even to this day. Compound binocular microscopes, as well as the monocular microscope (shown in Fig. 1), were routinely manufactured.

In this evolutionary process certain design constraints or constants became embodied in all microscopes. These included tube lengths on the order of 160 mm, binocular interpupillary distances on the order of 60 mm, and a definition of magnification as [5]

$$M = \frac{250 \text{ mm}}{(\text{equiv. focal length of magnifiers in mm})}.$$

These three values (160 mm, 60 mm, and 250 mm) each represented the recognition that the microscopes were to be used by humans. That is, the receiver of the magnified image was the human visual system with a relaxed accommodation distance for a real object of about 250 mm, an interpupillary dis-

0018-9294/82/0200-0070$00.75

tance of about 60 mm, and a physical body size that made a 160 mm tube length convenient.

Even as the types of different microscopy expanded from reflectance and brightfield to include darkfield, phase, interference, polarization, and fluorescence, these parameters and one other remained fixed in the design of microscope imaging systems.

II. Resolution and Acuity

For our purposes we shall use the Rayleigh criterion that defines the resolution limit of an optical system on the basis of the overlapping of two Airy disks (Fig. 2). That is, two "point objects" imaged from infinite onto a plane will each produce a diffraction image (in intensity) of

$$I(r) = \{2J_1(r)/r\}^2 \tag{1}$$

where r is radial distance from the center of the circularly symmetric optical system and $J_1(r)$ is a first-order Bessel function [6].

A common definition of the resolving limit R of an optical microscope system is in terms of a smallest distance r' such that $I(r') = 0$. From Fig. 2 and the definitions of r' and R in terms of the parameters of the optical system [6] we have

$$3.832 = r' = (2\pi/\lambda)\,(\mathrm{NA})\,R$$

or

$$R = \frac{0.61\lambda}{\mathrm{NA}} \tag{2}$$

where NA is the numerical aperture of the lens and λ is the wavelength of incoherent illumination. We shall choose the wavelength to be $\lambda = 0.492\,\mu$ (blue/green light) so that the resolution limit will be $R = 0.3/\mathrm{NA}\,\mu$. We may invert this expression to yield a resolution limit in points/μ as $P = \mathrm{NA}/0.3$. For conventional microscope systems P may vary from 0.4 points/μ (5X objective) to 4.4 points/μ (oil-immersion objective).

In terms of the human engineering of microscope systems we might now ask, "How many resolvable points are there (or should there be) across a microscope field-of-view?" The answer may be found by looking at the acuity characteristics of the human visual system which, with a resolution of approximately 1′ of arc when focused at infinity, is capable of resolving approximately 800–1000 points across the visual field [7]. As we shall see in data that will be presented shortly, this parameter has also been embodied in the design of microscope lenses.

III. Reinventing the Microscope

What if the human were not the receiver of the image produced by a microscope? What if the image were to be quantitatively processed by a computer to produce a record of a field-of-view, measurements on the objects in a field-of-view, or a judgement of the normalcy of the objects seen in a field-of-view? These are the questions that have confronted us as we have developed a new microscope system for the automated quantitative analysis of microscopic images. The primary use of this system is to be in the biomedical field and the design parameters have been chosen accordingly. We believe, however, that such an instrument will have a broad range of applications in such fields as powder metallurgy, geology, and semiconductor fabrication technology.

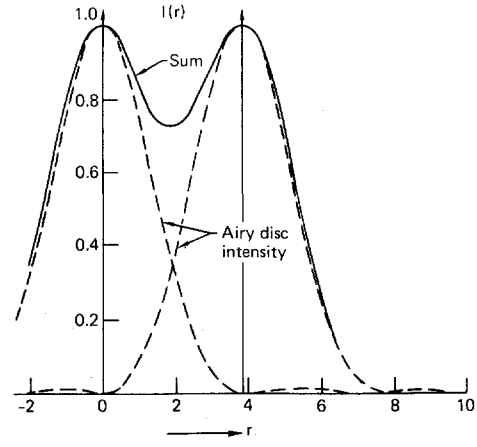

Fig. 2. Intensity sum of two Airy disks. The definition of the resolving limit (see text) places the maximum of each above the first zero of the other (from [6]).

A. The Specifications

Over 40 years ago Caspersson [8], [9] performed the pioneering work that demonstrated the use of quantitative and objective analysis of data contained in a microscope image. While his was an interactive procedure, the actual measurements were made through a microscope on single cells by instrumentation rather than human visual estimation. The development of modern electronics, particularly electrooptical scanners and digital computers, that followed World War II provided the technology necessary for the automated scanners of the early 1960's. These scanners made faster acquisition of cytologic image data possible and thus fostered a range of projects in image cytometry including exfoliative cytology [10]–[14], automated leukocyte recognition [15]–[20], and automated karyotyping [21]–[25]. Although the results were not always spectacular, nevertheless a fund of knowledge was built up that pointed the way to better mechanisms for the acquisition, description, measurement, and interpretation of data derived from automated cell image analysis.

While the list of those who have worked and published in this field is exceedingly long and almost encyclopedically covered in [26] and [27], a few results that serve as key features for our system should be mentioned here. Bacus [28], Green [29], Kruse [30], and Zack [31] have shown that a sampling density of about 0.5 μ is necessary and sufficient for the analysis of erythrocyte morphology. Bacus [32], Young [33], [34], Brenner [35], Prewitt [19], Ingram [36], and Tyko [37] have also seemed to confirm this figure for leukocyte analysis. In the analysis of exfoliative cervical cytology Bartels [38] has shown through careful studies that 0.5 μ sampling is necessary for accurate cell classification. Photometric errors that may occur when cells are sampled too coarsely have been studied and described by Ornstein [39], Mayall [40], Prewitt [41], and Mendelsohn [42]. Analyses have also shown that a brightness resolution of 256

levels (8 bits) is adequate for biological imaging. To achieve a resolution of 256 levels a signal-to-noise ratio (SNR) of about 512:1 is necessary. Here we measure full scale signal strength against rms noise. For example, if the full scale signal were 1 V, then to achieve 512:1 SNR the rms noise voltage should be less than 2 mV. In certain applications where optical density is to be measured, the required SNR may, in fact, be much higher. We shall concentrate our attention, however, on the specification in terms of brightness resolution.

In summary, a sampling density less than 2 picture elements (pixels)/μ is too coarse with respect to both photometric and spatial information; sampling greater than 2 pixels/μ is costly, of limited value, and only possibly required in chromosome analysis [25]. Brightness resolution should be 8 bits.

For both clinical and research applications it has been shown that overall throughput rates require slide processing times of less than 3 min [43]. If we use a 1 X 1 cm total examination field on a slide specimen with 2 pixels/μ sampling density (and resolution), we see that the total number of pixels/slide to be scanned and processed is $N = 4 \times 10^8$ pixels/slide. With a total of, say, 200 s available to scan and subsequently process the slide, this means that a data acquisition rate higher than 2×10^6 pixels/s must be attained.

Our solution for a microscope system that would simultaneously meet all of these specifications is a high-resolution, wide-field, high-speed, and high-SNR electrooptical system. A key design feature is the concept of the wide-field, high-resolution microscope. In image cytometry one of the problems frequently encountered is the edge effect associated with the field-of-view size. Consider the field-of-view shown in Fig. 3. The total field width D is presumed to contain cells of average diameter "d" that we wish to analyze for a variety of properties including size, shape, and optical density.

Unfortunately, some of these cells will be on the border of the field-of-view, and hence measurements made on them will be faulty. This means that a region around the border of the picture of width "d" must be discarded. The *effective* area of the field-of-view is therefore reduced from D^2 to $(D - 2d)^2$. The percentage of area lost from the original field may be expressed as

$$\text{percent lost} = \frac{D^2 - (D - 2d)^2}{D^2} \times 100 \text{ percent}$$

$$= \left[1 - \left(\frac{D - 2d}{D}\right)^2\right] \times 100 \text{ percent}.$$

After a little algebra this becomes

$$\text{percent lost} = 4(d/D)(1 - d/D) \times 100 \text{ percent}. \quad (3)$$

With d fixed at, say, 20 μ and a field-of-view of $D = 200$ μ, the percentage area lost is 36 percent. With a field-of-view of 2000 μ, however, this drops to 3.96 percent. Clearly, there is a big payoff in scanning the largest possible field at the required resolution. One alternative, an expensive one, is to mechanically move the specimen after the scan of a small field-of-view (say, 200 μ) so that the next scanned field is precisely aligned with the previous one. Thus, cells on the common border are not "lost." This requires a stage motion

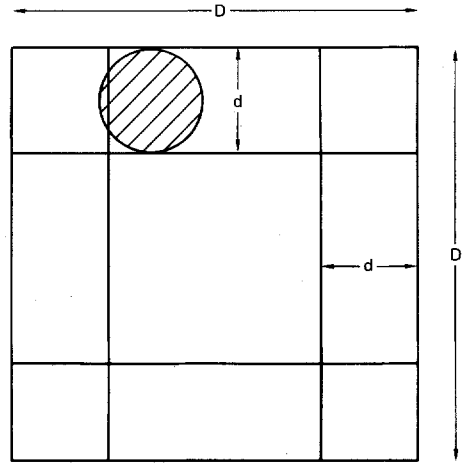

Fig. 3. Model for the computation of area lost from a field-of-view due to border touching cells of a given diameter.

that is both fast and accurate to within half a pixel spacing. Such mechanical stages exist but are prohibitively expensive and also quite bulky.

Another alternative is to move the specimen in a smooth, continuous motion beneath a conventional microscope lens with 2 pixels/μ resolution and a field diameter of perhaps 500 μ (see Fig. 6). Such a system can be constructed with currently available technology and represents one possible design approach.

Our design approach follows still another path and is based upon the use of a wide-field lens that simultaneously has a resolving power of about 2 pixels/μ and a field-of-view of 2000 μ, that is, 2 mm.

Matched to a linear, charge-coupled photodiode array of length 2048 as shown in Fig. 4, two-dimensional scenes may be scanned by means of a galvanometer-driven mirror. To cover a 1 X 1 cm total area on a slide specimen, 50 fields-of-view, each 1 mm (~2048 pixels/row) X 2 mm (~4096 rows) are required. To move from one field-of-view to another a simple mechanical stage may be used that need not have the mechanical resolution previously described. Instead, each step can be a coarse 1.1 or 2.1 mm with no attempt made to align the common borders of pictures. We can afford this approach because our field-of-view is sufficiently large that we do not suffer from the few percent of area lost at the field borders.

The effect of having a wide-field lens on the rate of cell image acquisition is summarized in Fig. 5. We assume that pixels are scanned at a rate of 5×10^6 pixels/s and that the sampling density is approximately 2 pixels/μ.

Because several of the subsystems are crucial to this performance of our microscope system, it is worthwhile to expand upon our discussion of them.

B. The Lens

The lens we have chosen was developed for use in the manufacture of integrated circuit photomasks. The lens, an Ultra-Nikkor 30 mm f/1.2e, has in the standard configuration a magnification of 25X so that a 2 mm object size becomes a 50 mm image size. To appreciate how this lens differs from ordinary microscope optics we performed a small experiment using a stage micrometer. The micrometer permits us to mea-

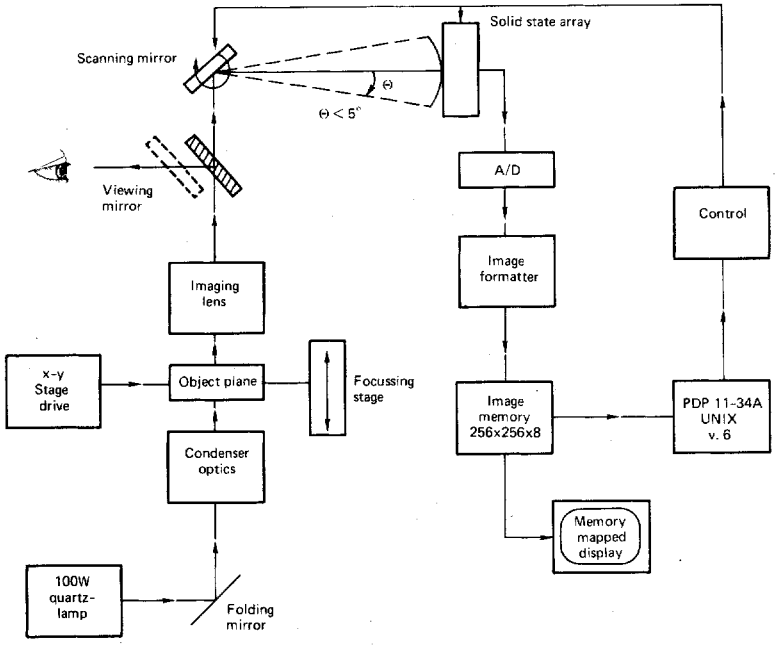

Fig. 4. System diagram for Solid-State Automated Microscope (SSAM).

	D = 5μ	D = 15μ	D = 50μ
Cells per picture	71000	7900	710
Cells per second	42300	4700	423
Time per cell	24μs	213μs	2400μs

Fig. 5. Cell image acquisition rates for various cell sizes. Cells are assumed to be tightly packed and their relative diameters are illustrated at the top of the figure. Typical cells corresponding to these diameters are red blood cells ($D = 5\ \mu$), white blood cells ($D = 15\ \mu$), and cervical cells ($D = 50\ \mu$). To facilitate comparison we note that a conventional lens with the same resolution but a field diameter of 400 μ would contain 5025, 558, and 50 cells corresponding to each of the three diameters.

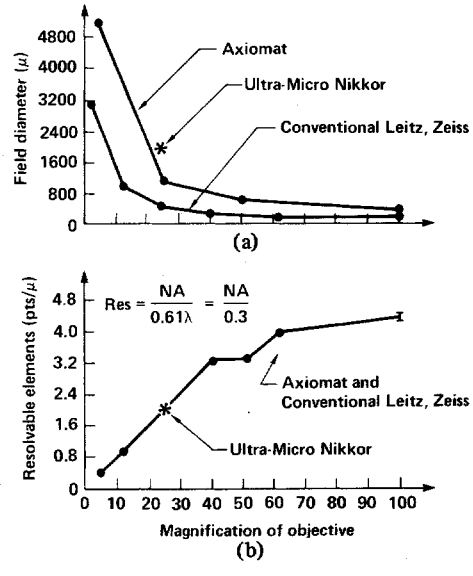

Fig. 6. (a) Field-of-view diameter (in microns) for various microscope objective/ocular lens systems. (b) Resolving power (in points/micron) for various lens systems. The value for the Ultra-Micro Nikkor is based on measured resolution rather than NA.

sure the field-of-view diameter associated with different power objective lenses and a fixed ocular lens. As shown in Fig. 6(a) for a variety of lenses and microscope systems, we see that as the magnification power of the objective increases, the field width decreases. In Fig. 6(b) we show for these same lenses their resolving power in points per micron as calculated from the numerical aperture by the procedure described in Section II.

We observe that as the magnification of the lens increases, the numerical aperture and the resolving power increase. In Fig. 7 we multiply the curves in Fig. 6(a) by the curve in Fig. 6(b) to produce curves that describe the total field width in resolvable points as a function of magnification for different lenses and microscope systems. Notice that for conventional microscope systems the number of resolvable points across a field diameter matches the resolution capability of the human visual system described in Section II.

We do not mean to imply that the Ultra-Micro Nikkor is the only lens that can achieve these specifications. In fact, several manufacturers including Zeiss and Olympus make lenses with similar characteristics. Compared to lenses used for *conventional* microscopy, however, Fig. 7 shows that this lens has extraordinary characteristics.

C. The Sensor

The optoelectrical transducer that we use is the Fairchild CCD1500 camera system built around a 2048 X 1 (linear) charge-coupled photodiode array, the Fairchild CCD143DC. Although our system can easily accommodate a linear array up to 4096 long, at the time of this writing this is the longest commercially available line-scan camera. As shown in Fig. 8 the array consists of a set of photodiodes that integrate the

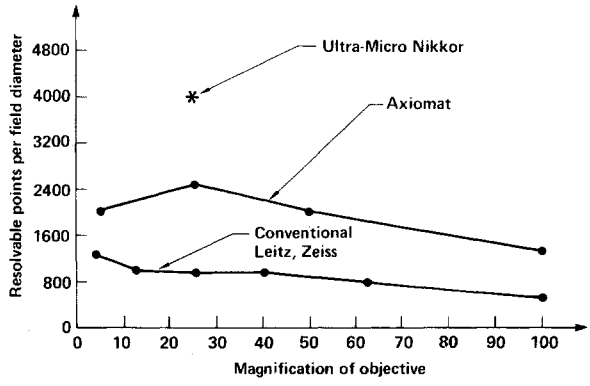

Fig. 7. Field-of-view diameter (in resolvable points) for various microscope lens systems.

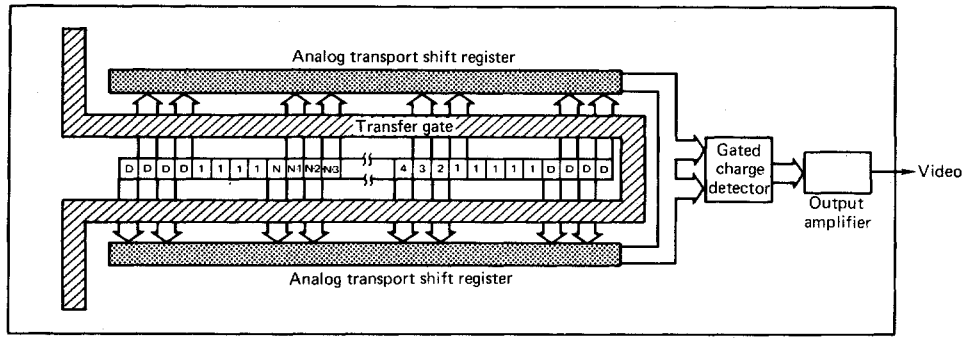

Fig. 8. System diagram of a linear, charge-coupled photodiode array. Note that even photodiode locations are handled by one shift register and odd photodiodes by a second shift register to reduce internal clock frequency requirements.

received light over a user selected time period and then transfer their charges into analog CCD shift registers.

While the line of analog data is being shifted out, a new integration interval is begun. The clock rate for the CCD is fixed at 5 MHz independent of the integration period indicating that a minimum integration period is (200 ns/pixel) X (2048 pixels/line) = 409.6 μs/line. The reason for fixing the CCD clock period is to guarantee that the charge transport characteristics are constant even when integration times are varied as, for example, in low light-level situations [44]. The individual photodiode elements are illustrated in Fig. 9.

The photodiode elements on 13 μ centers are equivalent to 0.46 μ photodiodes on the object plane when placed at the image plane of the lens. The spectral sensitivity of the photodiodes is essentially flat over the useful spectral range of the lens, that is, 0.510 μ (green) to 0.570 μ (yellow). The measured peak-to-peak noise/photodiode is less than 1 mV with a full scale signal of 1 V, and thus the SNR (as defined earlier) exceeds 1000:1 (60 dB) at room temperatures.

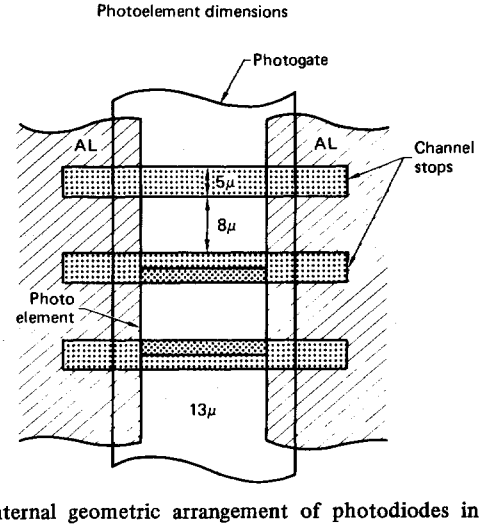

Fig. 9. Internal geometric arrangement of photodiodes in the linear array.

D. Other Components

While most of the mechanical components of the system are built from standard Zeiss microscope components (for example, the stage, focusing body, and condenser), two of the subsystems are worth discussing in a little greater detail.

1) The Galvanometer Scanner: The mirror scanner, shown diagrammatically in Fig. 4, is a General Scanning G-300PD scanner and a CCX-100 servocontroller. The mirror position is driven by a 12 bit counter through a D/A converter to select sequentially 4096 different lines. With the height of each line on the object plane being 0.46 μ, this represents a total scan height of 1888 μ, a figure slightly less than the field diameter of the lens. The total deflection angle is slightly less than 10° and the shortest time in which this angle is swept out is (4096

lines/picture) × (409.6 μs/line) = 1.678 s/picture. Thus, the angular velocity of the mirror is 0.10 rad/s, a modest amount. The angular resolution required of the mirror scanner is given by 10°/4096 or 8.8″ of arc/line. The resolution available in the sequential mirror scanning system is 1″ of arc. A greater problem in the scanner is bearing noise which may be as bad as 20″ of arc. This type of noise manifests itself as vertical blurring in the image. One potential solution to this problem that we are currently investigating is the use of the new GF-300PD scanner in place of the G-300PD. The newer version employs a flexure pivot instead of a ball bearing pivot, and thus bearing noise is reduced to zero.

2) The Illuminator: To provide adequate specimen illumination we use a 100 W quartz-halogen incandescent light source with a dc stabilized power supply and a 546 nm bandpass (*e*-line) filter. At the shortest integration time the amount of light available is sufficient to give a full scale (1 V) signal out of the photodiode array in background regions of a slide. The condenser illumination system uses Kohler illumination [45].

E. Electronic Processing

The analog video signal derived from the sensor is sampled and quantized using a TRW 8 bit A/D converter (Model TDC1007J) with conversions occurring every 200 ns. Through a custom-designed interface the 5 000 000 pixels/s are packed two to a 16 bit computer word and prepared for DMA transfer into our PDP11-34A computer. The rectangular 2048 × 4096 picture is obviously too large to fit in the memory of the PDP11-34A, so the interface provides the ability to choose either a 256 × 256 window (that is, a subset) from the entire picture or a 256 × 256 coarse representation of a 2048 × 2048 square view. This latter representation is obtained by averaging an 8 × 8 neighborhood of points into a single pixel. Since the minimum line time is 409.6 μs and only 128 words/line are actually transferred under DMA control into the computer, more than enough time per word is available for the data transfer. The actual memory used for picture storage is also shared between the PDP11-34A and a memory-mapped display system [46], [47], as shown in Fig. 4. The display is capable of showing either one of two pictures stored in a reserved 65 536 words of memory on the PDP-11 UNIBUS. Pictures acquired through the microscope and stored in memory are 256 rows × 256 columns × 8 bits, and thus use half of the reserved memory. All of the pictures that were scanned and digitized through this Solid-State Automated Microscope system (SSAM) and are presented in this paper were photographed off the display monitor of this memory-mapped display. The computer software chooses the starting upper-left coordinates (x, y) of the window, transmits this pair of 12 bit numbers to the interface, and the 256 × 256 picture then is scanned, digitized, and stored in memory.

The integration period for each line of video data is also software selectable from the computer and may range from a minimum of 410 μs/line to a maximum of 99.999 ms/line (5 BCD digits). At room temperatures it is not practical to use integration times greater than 100 ms/line due to dark current considerations. That is, at room temperatures the CCD wells will fill in 100 ms from the electrons produced by thermal agitation rather than incident photons.

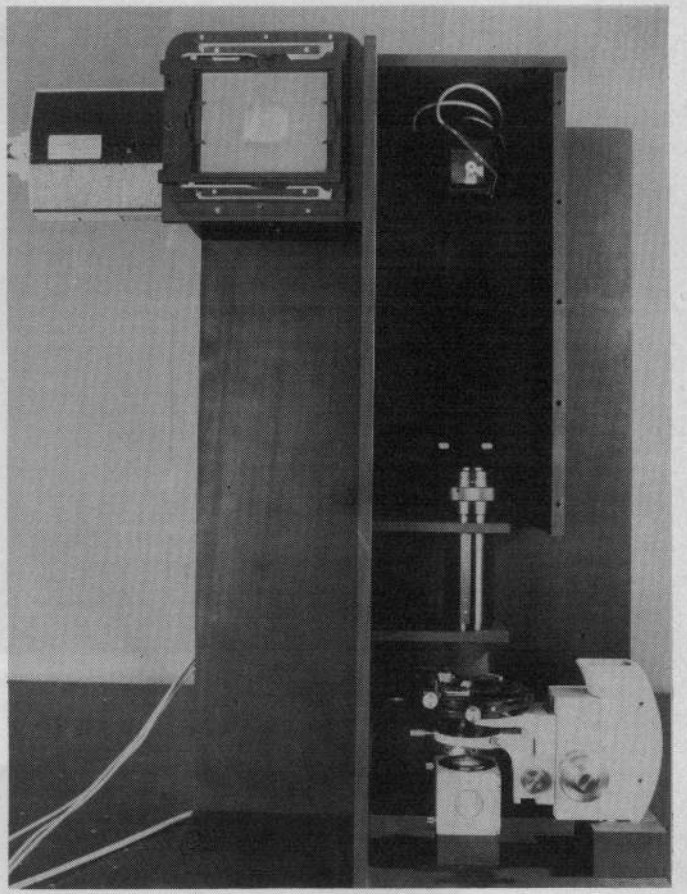

Fig. 10. Solid-State Automated Microscope System (SSAM). The control electronics are not shown.

F. The Completed System

The entire system is built on $\frac{1}{2}$ in stress-relieved aluminum and is shown in Fig. 10.

The control electronics occupy a standard 19 in wide cabinet and are approximately 24 in high and 27 in deep. If we were to repackage the control electronics this figure would change to about 11 in high and 30 in deep.

IV. System Performance

The testing and validation of our design specifications have been a most important part of our work. The fundamental problem is one of finding resolution test charts that would enable us to determine total system performance, that is, spatial resolution, brightness resolution (SNR), field-of-view coverage, etc. The availability of certain test microscope slides has helped us greatly in this. These slides are a stage micrometer (Leitz Corp.) and slide-based resolution and density test chart (Opto-Line Multidensity Resolution Target). On this latter slide a bar chart pattern is repeated at varying optical density levels ranging from 0.2–2.0. The bars themselves range from 10 line-pairs/mm to 500 line-pairs/mm. One of the test patterns is shown in Fig. 11.

A. Sampling Density

The sampling density, that is, the number of pixels/μ, was determined through the use of a stage micrometer. Bars on the micrometer as shown in Fig. 12 are separated by 10 μ.

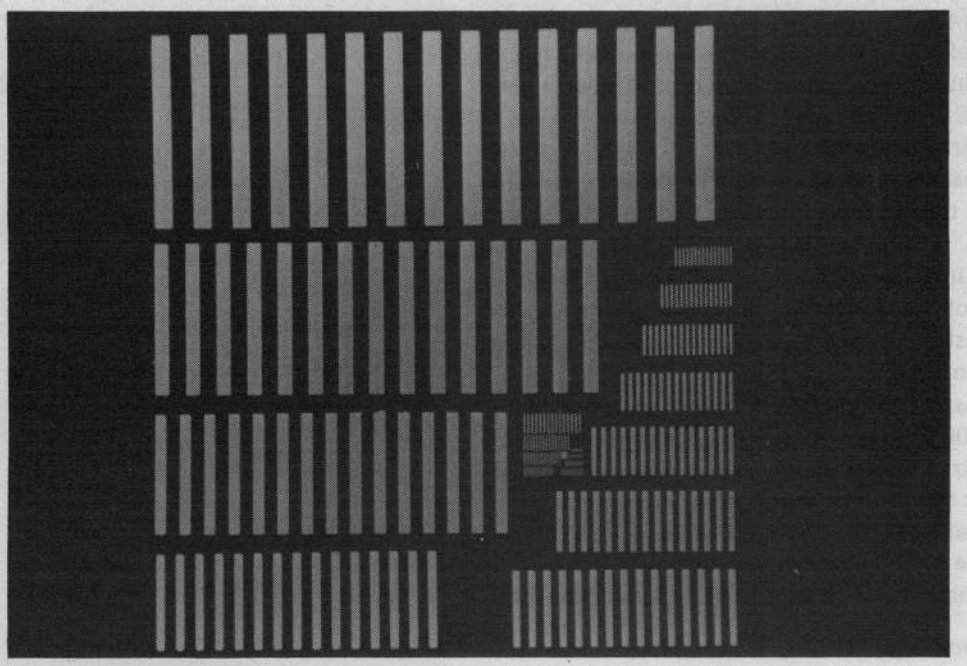

Fig. 11. Bar chart test pattern. The finest lines are 1 μ wide (500 line-pairs/mm) and bars increase in spacing by the tenth root of ten.

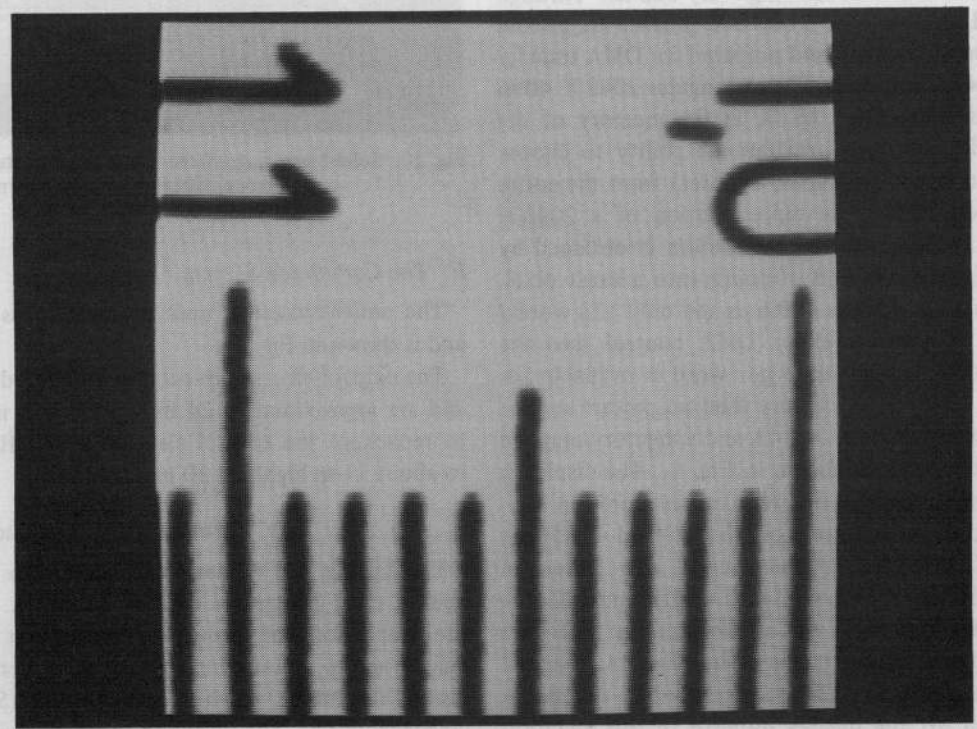

Fig. 12. Portion of stage micrometer image as viewed through SSAM. The distance between bars is 10 μ and the total picture width is 256 pixels.

By measuring the average number of pixels separating the bars we compute the sampling density to be 21.7 pixels/10 μ or 2.17 pixels/μ. Alternatively, this can be expressed as 0.46 μ/pixel. From this figure and knowledge of the photodiode array geometry (shown in Fig. 9) we can determine that the actual magnification of our lens configuration is (13 μ/0.46 μ) = 28.2×. The additional magnification, beyond the 25× associated with the lens itself, is due to the linear array being slightly further from the lens than the position of the design image plane. The design distance of the lens from the exit aperture to the image plane is 592.2 mm; in our system this distance is 667 mm.

B. Signal-to-Noise Ratio, Dynamic Range, and Tonal Transfer

In order to measure the signal-to-noise ratio (SNR) the following technique was employed. A clear field image of

256 X 256 was recorded with the galvanometer scanner turned off. Thus, the same line of image data was scanned 256 times and along any given column of the image the numerical value of the digitized brightness should have been the same. Due to noise sources in the image acquisition chain this was not the case. By measuring the rms value of the image brightness down any given column we computed the rms noise value. For 8 bits of brightness quantization (256 brightness levels), the rms value is 0.54 and the estimated SNR is (255/0.54) = 472:1 or 53.5 dB. This figure is in good agreement with the TRW specification for the SNR at the *output* of the A/D converter which is 54 dB [48]. The dynamic range of brightnesses in the original image that can be handled by SSAM is principally a function of the SNR at the *input* to the A/D converter. With an SNR in excess of 60 dB this means that a range of 1000:1 is possible. For low-light level signals the integration period may be varied over a range of 240:1 to increase the dynamic range until the dark current becomes a significant factor. We have also observed that there are deterministic variations in the pedestal voltage and signal gain from photodiode to photodiode, particularly between the even and odd photodiodes (see Fig. 8). With the galvanometer scanner off, these appear as vertical stripes in the image of what should be a clear field. These can be eliminated in software (or hardware) by measuring the response to a black field $B[i]$, the response to a white field $W[i]$, storing gain and offset correction factors as a function of photodiode position ($G[i]$, $0[i]$ $i = 0, 1, 2, \cdots, 2047$), and applying these factors as follows:

$$b[i] = G[i] * b[i] - 0[i] \qquad i = 0, 1, 2, \cdots, 2047. \tag{4}$$

The recorded brightness from photodiode number i for any subsequent image is $b[i]$ and the gain and offset correction for position i are given by

$$G[i] = \frac{255}{W[i] - B[i]}$$

$$0[i] = \frac{255 * B[i]}{W[i] - B[i]}.$$

For our particular camera system we have found that $G[i] \simeq 1$ and most of the correction is for offset errors. The result of applying this algorithm to an image obtained with the galvanometer scanner turned off is shown in Fig. 13.

After the correction described in (4) is applied, the tonal transfer characteristic of the entire system is linear from the light source to the computer memory. Thus, multiplication of the light or the transmissivity of the cellular specimen (at any specific location) by a constant factor will multiply the sampled and quantized brightness stored in computer memory by that same factor.

C. Contrast Modulation Transfer Function (CMTF)

The contrast modulation function is a measure of how the contrast existing in a test pattern is degraded as a function of the spatial size in the pattern. In our example (Fig. 11) the bar chart is deposited on the glass slide with a specified foreground/background optical density relationship. This density may be related to contrast as follows. The intensity measured

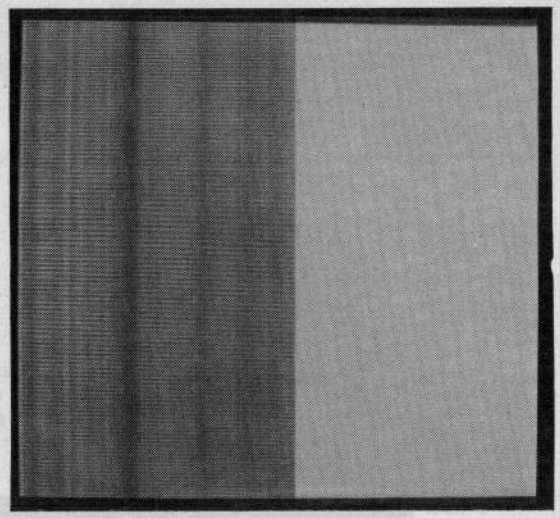

Fig. 13. Result of applying software compensation for variations in gain and offset across photodiodes. Left side is image before compensation; right side is image after compensation.

through the clear portions of the bar chart is the background illumination which we shall denote as I_{max}. The intensity measured through the darkened portions of the bar chart is decreased from the background illumination and is I_{min}. The relationship between these two quantities is given by the Beer-Lambert law

$$I_{min} = I_{max}\, 10^{-d}$$

where d is the optical density at the point of interest. The contrast is given by [49]

$$c = \frac{I_{max} - I_{min}}{I_{max} + I_{min}} \tag{5}$$

and by direct substitution this can be written as

$$c = \frac{1 - 10^{-d}}{1 + 10^{-d}}. \tag{6}$$

For example, where the optical density $d = 1.3$ (95 percent of the incident light is absorbed), $c = 0.90$. This is, of course, the contrast that would be measured either in large open regions of the test pattern where spatial variation was virtually nonexistent or with an electrooptical system with unlimited spatial resolution. Due to finite resolution, however, we observe a degradation in the contrast. This degradation as a function of spatial size is the contrast modulation function and in terms of line spacing on the bar chart is given by

$$c(l) = \frac{I_{max}(l) - I_{min}(l)}{I_{max}(l) + I_{min}(l)} \tag{7}$$

with l ranging from $l = 0$ line-pairs/mm (open regions) to $l = 500$ line-pairs/mm. For our system this function was measured from the digitized and quantized image stored in computer memory and the result is plotted in Fig. 14.

Ten different experimental contrast modulation function curves for ten different values of d in the range ($0.2 <= d <= 2.0$) were measured as defined in (7). When they were nor-

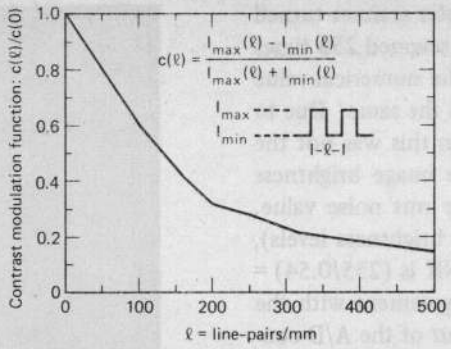

Fig. 14. Normalized contrast modulation function for the bar chart test pattern. The ideal contrast response is $c(0)$ and for our test pattern this number is given by manufacturer's specifications as ranging from $c = 0.23$ ($d = 0.2$) to $c = 0.98$ ($d = 2.0$).

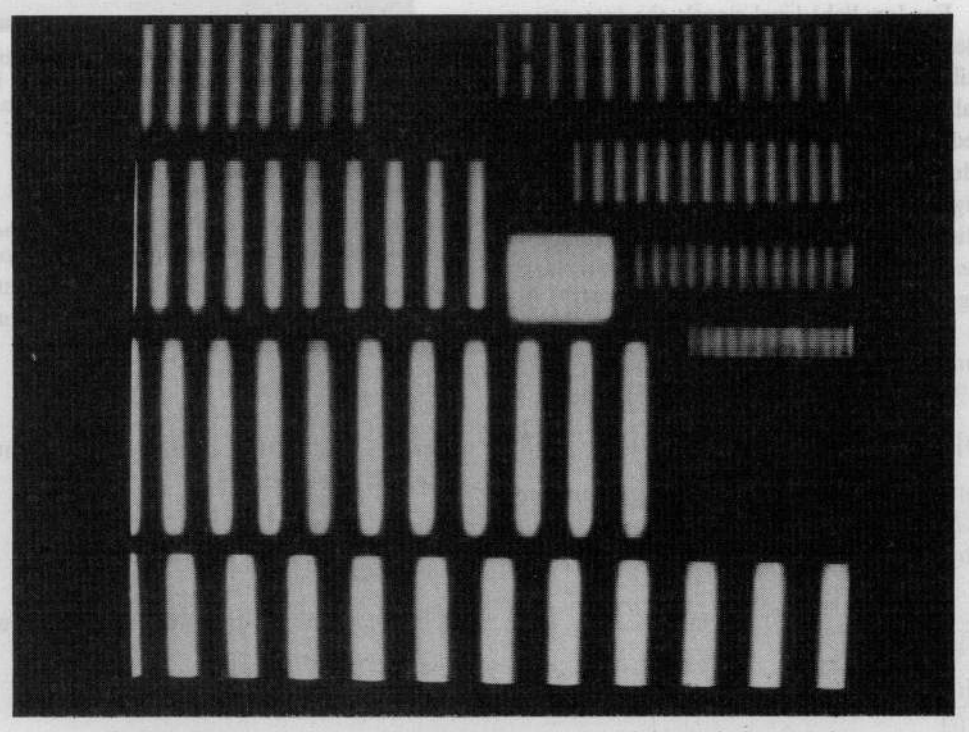

Fig. 15. Full resolution scan of the innermost portion of the resolution test chart.

malized by $c(0)$ they all gave the same result, that depicted in Fig. 14.

Another way to observe the degradation in the contrast as the line spacing decreases is to look at the actual digitized and quantized picture output as stored in computer memory. In Fig. 15 we see that as the line spacing approaches 500 line-pairs/mm, the contrast decreases but the bar pattern itself remains observable. Thus, we still at this value have not yet reached the resolution limit at which the bar pattern is no longer measurable.

D. Fourier Modulation Transfer Function (MTF)

The classical modulation transfer function based upon Fourier transform techniques may be evaluated in several ways. One technique is to measure the Fourier transform of the step response of the imaging system from the central square of the test pattern (Figs. 11 and 15) and compare this to the transform of the ideal step response. Another way is to view the bar chart test pattern as producing input "signals" with known frequency components. A similar technique that we have adopted is to use a mathematical mapping from the contrast modulation curve given in Fig. 14 to the classical MTF curve [50], [51]. Once again the computations were based upon the digitzed and quantized image stored in computer memory and the results are shown in Fig. 16.

While at first glance the MTF at 500 cycles/mm may not be overly impressive, we must point out that this is the MTF over the entire 2 mm diameter field-of-view, not just the central portion.

E. Biological Specimens

In this section we show several of the biological images acquired through SSAM. Fig. 17(a) shows part of a transverse section of a cat's brain stem. This particular image was

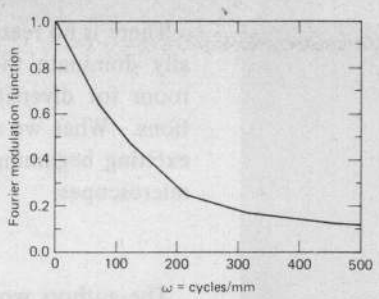

Fig. 16. Modulation transfer function (MTF). The magnitude of the complex Fourier spectrum of the complete system versus frequency in cycles/mm.

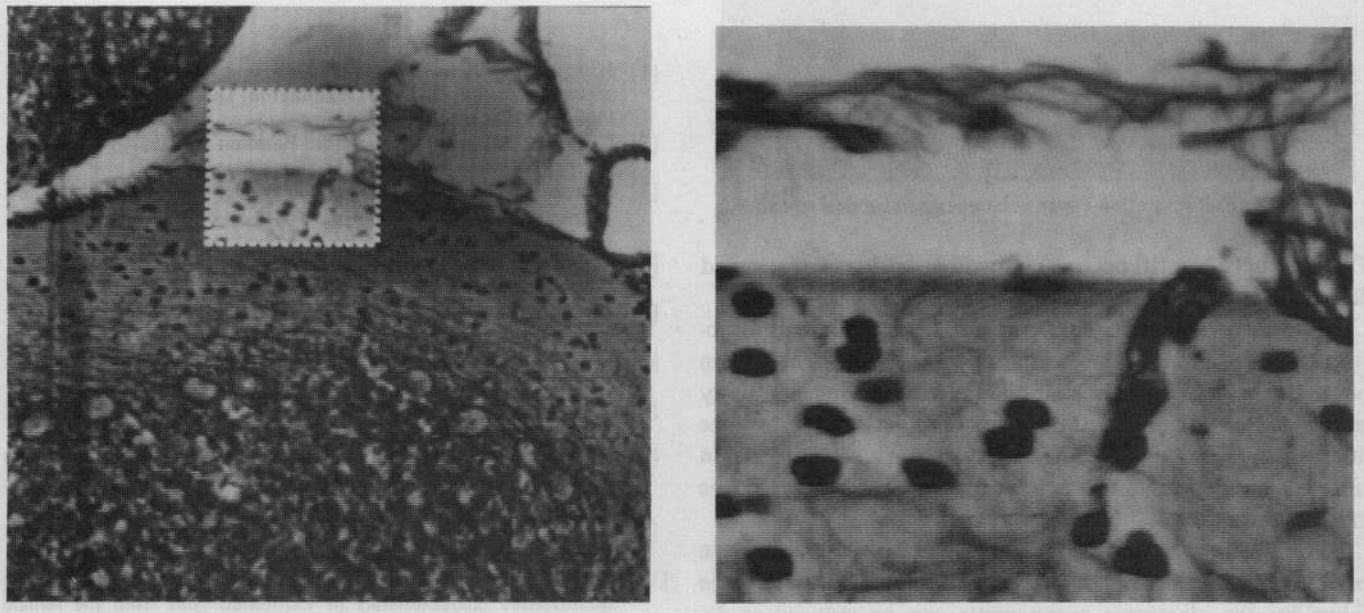

(a) (b)

Fig. 17. Transverse section of a cat's brain stem. (a) Reduced display to show part of the wide-field coverage of lens. Boxed portion corresponds to a 256 × 256 full resolution picture. (b) Full resolution image contained in box.

scanned at full resolution and then reduced for display purposes, as described in Section III-E. The field-of-view covered by the checkered box in the photo corresponds to the full resolution 256 X 256 picture that is shown in Fig. 17(b).

Fig. 18 shows another biological specimen of particular interest to our research effort in analytical cytometry.

V. Summary and Conclusions

We have developed the specifications and operating parameters for SSAM and described the measurement procedures and results used to verify our design goals for sampling density, signal-to-noise ratio (SNR), dynamic range, tonal transfer, and spatial resolution. An important aspect of our measurement procedure has been to characterize the complete system from the illumination source through to the computer memory. Thus, measurements include all sources of degradation, digital as well as analog. We have noted that the spectral response of the system is limited to the range 510 nm–570 nm. This is an inherent characteristic of the lens and thus constrains us in our use of the system. For most of the studies we plan with this system this constraint should not be too severe; a variety of biological stains, many of them stoichiometric, are available that are strongly absorbent in this spectral region. Other criteria for assessing the effectiveness of SSAM, such as data rate, size, versatility, and maintainability are issues of design. The first two of these have been discussed in Sections III-E and III-F, but some further discussion is appropriate.

The rate at which pixels are acquired (5×10^6 pixels/s) with 8×10^6 pixels/picture makes it clear that it is inappropriate to think of storing the entire image in a computer memory. Indeed, the slide itself should be viewed as the memory with SSAM serving as the fast data bus to a CPU. The short amount of time available per pixel (200 ns) indicates that we must be quite careful about what sort of real-time processing is proposed. We should view processing "on-the-fly" as akin to taking a drink from a fire hose; extreme care is required. At the present time, however, there are a number of algorithms that provide reasonable scene segmentation and cell measurement in something approaching one pass through the picture.

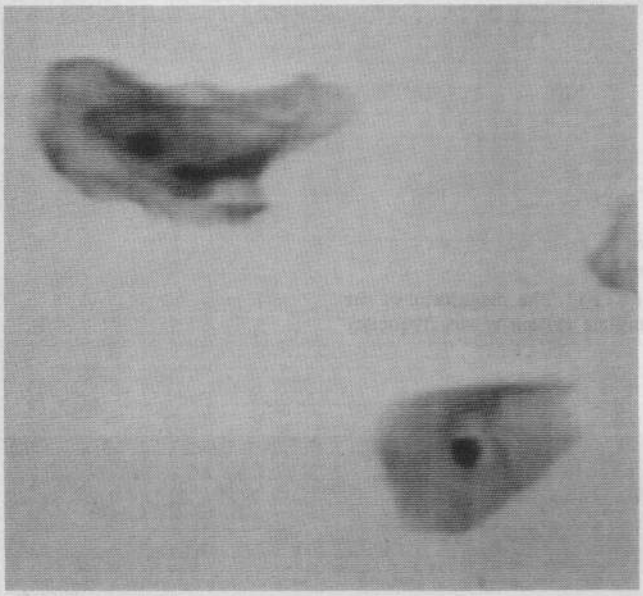

Fig. 18. Full resolution Papanicolaou-stained cervical smear.

That is, these algorithms are compatible with raster scanned devices [52]-[56].

Our present system is configured for transillumination absorption microscopy. Due to the open portion of the system between the lens and the scanning mirror, it would be fairly simple to reconfigure SSAM for epi-illumination fluorescence microscopy. In this case the ability to vary the integration time to permit adequate photoelectron integration would be extremely important.

The possibility exists for reducing the present physical size of SSAM in its electronic and optical components. The space taken by the electronic components can be reduced as described earlier. The physical space occupied by the optical components could be reduced by designing a folded optical path. A further improvement in performance relative to size will occur when linear CCPD arrays of 4096 are available.

The design and use of widefield microscopes should make a significant impact on quantitative microscopy in the coming years. We are not the only group that has been involved in the design of a microscope that is tuned to the capabilities of modern, computerized, quantitative image processing. Zahniser *et al.* [57] have used an Ultra-Micro Nikkor lens (28 mm, f/1.7e), which has a field-of-view coverage of 8 mm with a resolution only 33 percent degraded from the one we have employed, to make photonegatives of cervical specimens. These photonegatives were then subsequently scanned by the BioPEPR system and analyzed for abnormal cells. Their work, performed at the University of Nijmegen, has been some of the most encouraging seen in recent years on automated cervical screening. Another important project has been proceeding in parallel with ours at the University of Arizona under the direction of Shack and Bartels [58]. Their system is essentially a widefield flying spot scanner that uses a laser source of illumination, a rotating polygonal mirror for x-direction scanning, and continuous mechanical stage motion for y-direction scanning. Their elegant solution represents a technological *tour de force.*

There is no reason to believe that any one design will eventually dominate the field. To the contrary, there is as much room for diversity in design as there is diversity in applications. What we do believe is that these systems represent an exciting beginning for a new generation of sophisticated light microscopes.

Acknowledgment

The authors would like to acknowledge the advice and help of their colleagues R. Jesse and J. Zumstein. Dr. B. Mayall also made substantial contributions to this work through discussions and critiques.

References

[1] H. R. Purtle, "History of the microscope," in *The Billings Microscope Collection*, 2nd ed. Washington, DC: Armed Forces Inst. Pathol., 1974, pp. x-xviii.

[2] C. Sagan, *Cosmos.* New York: Random House, 1980, ch. VI, pp. 137-149.

[3] I. Asimov, *Asimov's Biographical Encyclopedia of Science and Technology*, rev. ed. Garden City, NY: Doubleday, 1972, pp. pp. 129-130.

[4] J. Grehn, *Leitz Microscopes for 125 Years.* Wetzlar, Germany: Leitz, Inc., 1977.

[5] L. C. Martin, *The Theory of the Microscope.* New York: Elsevier, 1966, ch. III, pp. 95-99.

[6] —, *The Theory of the Microscope.* New York: Elsevier, 1966, ch. III, pp. 95-99.

[7] G. M. Murch, *Visual and Auditory Perception.* Indianapolis, IN: Bobbs-Merrill, 1973, ch. 3, pp. 77-82.

[8] T. Caspersson, "Uber den chemischen aufbau der strukturen des zellkernes," *Skand. Arch. Phys.*, vol. 73, suppl. 8, pp. 1-151, 1936.

[9] —, "RNA in both nucleus and cytoplasm, and the function of the nucleolus," *Proc. Nat. Acad. Sci.*, vol. 26, p. 507, 1940.

[10] W. E. Tolles, W. J. Horvath, and R. C. Bostrom, "A study of the quantitative characteristics of exfoliated cells from the female genital tract: I. Measurement methods and results," *Cancer*, vol. 14, no. 3, pp. 437-454, May-June, 1961.

[11] —, "A study of the quantitative characteristics of exfoliated cells from the female genital tract: II. Suitability of quantitative cytological measurements for automatic prescreening," *Cancer*, vol. 14, no. 3, pp. 455-468, May-June, 1961.

[12] G. L. Wied, P. H. Bartels, G. F. Bahr, and D. G. Oldfield, "Taxonomic intra-cellular analytic system (TICAS) for cell identification," *Acta Cytol.*, vol. 12, pp. 180-204, 1968.

[13] G. L. Wied, G. F. Bahr, D. G. Oldfield, and P. H. Bartels, "Computer assisted identification of cells from uterine adenocarcinoma. Clinical feasibility study with TICAS. I. Measurements at wavelength 530 nm," *Acta Cytol.*, vol. 12, pp. 357-370, 1968.

[14] —, "Computer assisted identification of cells from uterine adenocarcinoma. Clinical feasibility study with TICAS. II. Measurements at wavelength 530 nm," *Acta Cytol.*, vol. 13, pp. 21-26, 1969.

[15] P. H. Bartels, G. F. Bahr, and G. L. Wied, "Cell recognition from scan line transition probability profiles," *Acta Cytol.*, vol. 13, pp. 210-217, 1969.

[16] M. Ingram and K. Preston, "Automatic analysis of blood cells," *Sci. Amer.*, vol. 223, pp. 78-82, 1970.

[17] B. H. Mayall, "Deoxyribonucleic acid cytomorphometry of stained human leukocytes: I. Differences among cell types," *J. Histochem. Cytochem.*, vol. 17, no. 4, pp. 249-257, 1969.

[18] K. Preston, "Machine techniques for automatic leukocyte pattern analysis," *Ann. N.Y. Acad. Sci.*, vol. 97, pp. 482-490, 1962.

[19] J. M. S. Prewitt and M. L. Mendelsohn, "The analysis of cell images," *Ann. N.Y. Acad. Sci.*, vol. 128, pp. 1035-1053, 1966.

[20] I. T. Young, "Automated leukocyte recognition," in *Automated Cell Identification and Cell Sorting*, G. L. Wied, Ed. New York: Academic, 1970.

[21] J. Hilditch and D. Rutovitz, "Chromosome recognition," *Ann. N.Y. Acad. Sci.*, vol. 157, pp. 339-364, 1969.

[22] R. S. Ledley and F. H. Ruddle, "Chromosome analysis by computer," *Sci. Amer.*, vol. 214, pp. 40–46, Apr. 1966.
[23] R. S. Ledley, "Automatic pattern recognition for clinical medicine," *Proc. IEEE*, vol. 57, no. 11, pp. 2017–2035, 1969.
[24] M. L. Mendelsohn, T. J. Conway, D. A. Hungerford, W. A. Kolman, B. H. Perry, and J. M. S. Prewitt, "Computer-oriented analysis of human chromosomes: I. Photometric estimation of DNA content," *Cytogenetics*, vol. 5, pp. 223–242, 1966.
[25] M. L. Mendelsohn, Ed., "Automation of cytogenetics," in *Proc. Asilomar Workshop*, Pacific Grove, CA, Nov. 1975.
[26] P. H. Bartels and G. L. Wied, "Computer analysis and biomedical interpretation of microscopic images: Current problems and future directions," *Proc. IEEE*, vol. 65, no. 2, pp. 252–261, 1977.
[27] K. Preston, "Digital image analysis in cytology," in *Digital Image Analysis*, A. Rosenfeld, Ed. New York: Springer, 1979.
[28] J. W. Bacus, M. C. Belanger, R. K. Aggarwal, and F. E. Trobaugh, "Image processing for automated erythrocyte classification," *J. Histochem. Cytochem.*, vol. 24, pp. 195–201, 1976.
[29] J. E. Green, "Computer methods for erythrocyte analysis," presented at IEEE Conf. Recog. Symp. Feature Extraction and Selection in Pattern Recog., 1970.
[30] B. Kruse, "Design and implementation of a picture processor," in *Linkoeping Studies in Science and Technology Dissertations No. 13*, Linkoeping, Sweden, 1977.
[31] A. G. Zack, I. T. Young, S. E. Sher, and M. S. Greenberg, "Quantitative analysis of morphologic changes in erythrocytes during kidney dialysis," presented at the 5th Eng. Found. Conf. Automat. Cytol., Pensacola, FL, Dec. 1976.
[32] J. W. Bacus and E. E. Gose, "Leukocyte pattern recognition," *IEEE Trans. Syst., Man, Cybern.*, vol. SMC-2, Sept. 1972.
[33] I. T. Young, "The classification of white blood cells," *IEEE Trans. Biomed. Eng.*, vol. BME-19, no. 4, pp. 291–298, 1972.
[34] I. T. Young and I. L. Paskowitz, "Localization of cellular structures," *IEEE Trans. Biomed. Eng.*, vol. BME-22, no. 1, pp. 35–40, 1975.
[35] J. F. Brenner, E. S. Gelsema, T. F. Necheles, P. W. Neurath, W. D. Selles, and E. Vastola, "Automated classification of normal and abnormal leukocytes," *J. Histochem. Cytochem.*, vol. 22, pp. 697–706, 1974.
[36] M. Ingram and K. Preston, "Automatic analysis of blood cells," *Sci. Amer.*, vol. 223, pp. 72–82, 1970.
[37] D. H. Tycko, S. Anbalagan, H. C. Liu, and L. Ornstein, "Automatic leukocyte classification using cytochemically stained smears," *J. Histochem. Cytochem.*, vol. 24, no. 1, pp. 178–194, 1976.
[38] P. H. Bartels and G. L. Wied, "High resolution prescreening systems for cervical cytology," in *The Automation of Uterine Cancer Cytology, Tutorials on Cytology*. Chicago, IL, 1976, pp. 144–167.
[39] L. Ornstein, "The distributional error in micro-spectrophotometry," *Lab. Invest.*, vol. 1, pp. 250–265, 1952.
[40] B. H. Mayall and M. L. Mendelsohn, "Deoxyribonucleic acid cytophotometry of stained human leukocytes: II. The mechanical scanner of CYDAC, the theory of scanning photometry and the magnitude of residual errors," *J. Histochem. Cytochem.*, vol. 18, pp. 383–407, 1970.
[41] J.M.S. Prewitt, "The selection of sampling rate for digital scanning," *IEEE Trans. Biomed. Eng.*, vol. BME-12, 1965.
[42] M. L. Mendelsohn, "Absorption cytophotometry: Comparative methodology for heterogeneous objects, and the two-wavelength method," in *Introduction to Quantitative Cytochemistry*, G. L. Wied, Ed. New York: Academic, 1966.
[43] Coulter Corp., The Corning Corp., and The Geometric Data Corp., personal communications.
[44] R. B. Bishop, "Modelling the charge transfer process in charge coupled devices," Ph.D. dissertation, Dep. Elec. Eng. Comput. Sci., Massachusetts Inst. of Technol., Cambridge, MA, Jan. 1980.
[45] L. C. Martin, *The Theory of the Microscope*. New York: Elsevier, 1966, ch. III, pp. 105–110.
[46] S. M. Goldwasser, "A high performance continuous tone display processor," S.M. thesis, Dep. Elec. Eng. Comput. Sci., Massachusetts Inst. of Technol., Cambridge, MA, 1976.
[47] D. H. Alsip, "An advanced color image display processor," S.M. thesis, Dep. Elec. Eng. Comput. Sci., Massachusetts Inst. of Technol., Cambridge, MA, June, 1979.
[48] TRW LSI Products, *Technical Specification Note for ADC TDC1007J*, Redondo Beach, CA, 1978, p. 2.
[49] H. P. Lavin, "System analysis," in *Photoelectronic Imaging Devices*, vol. 1, L. M. Biberman and S. Nudelman, Eds. New York: Plenum, 1971, pp. 333–374.
[50] J. A. Hall, "Evaluation of signal-generating image tubes," in *Photoelectronic Imaging Devices*, vol. 2, L. M. Biberman and S. Nudelman, Eds. New York: Plenum, 1971, pp. 77–115.
[51] I. Limansky, "A new resolution chart for imaging systems," *Electron. Eng.*, pp. 50–55, June 1968.
[52] I. T. Young, R. L. Peverini. P. W. Verbeek, and P. J. van Otterloo, "A new implementation for the binary and Minkowski operators," *Comput. Graphics Image Processing*, vol. 17, pp. 189–210, Nov. 1981.
[53] A. Rosenfeld and A. C. Kak, *Digital Picture Processing*. New York: Academic, 1976.
[54] F. Veillon, "One pass computation of morphological and geometrical properties of objects in digital pictures," *Signal Processing*, vol. 1, pp. 175–189, July 1979.
[55] R.L.T. Cederberg, "Chain-link coding and segmentation for raster scan devices," *Comput. Graphics Image Processing*, vol. 10, pp. 224–234, July 1979.
[56] J. E. Green, "Rapid analysis of hematology image data–The ADC-500 preprocessor," *J. Histochem. Cytochem.*, vol. 27, pp. 174–179, Jan. 1979.
[57] D. J. Zahniser, P. S. Oud, M.C.T. Raaijmakers, G. P. Vooys, and and R. T. van de Walle, "BioPEPR: A system for the automatic prescreening of cervical smears," *J. Histochem. Cytochem.*, vol. 27, pp. 635–641, Jan. 1979.
[58] R. Shack, R. Baker, R. Buchroeder, D. Hillman, R. Shoemaker, and P. H. Bartels, "Ultrafast laser scanner microscope," *J. Histochem. Cytochem.*, vol. 27, pp. 153–159, Jan. 1979.

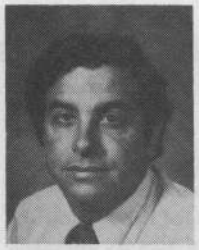

Ian T. Young was born in Chicago, IL, on December 15, 1943. He received the B.S., M.S., and Ph.D. degrees, all in electrical engineering, from the Massachusetts Institute of Technology, Cambridge, in 1965, 1966, and 1969, respectively.

From 1969 to 1973 he was an Assistant Professor of Electrical Engineering and from 1973 to 1979 he was an Associate Professor of Electrical Engineering at M.I.T. From 1978 to 1981, he was a Group Leader for Pattern Recognition and Image Processing in the Biomedical Sciences Division of Lawrence Livermore National Laboratory, University of California, Livermore. He has been a Visiting Professor in the Electrical Engineering Departments of the Technical University Delft, The Netherlands, in 1975–1976, the Technical University Linkoping, Sweden, in 1976, and the Ecole Polytechnique Federale de Lausanne, in 1979–1980. Over the past decade he has been a Consultant to a number of companies including M.I.T's Lincoln Laboratory and the Coulter Biomedical Research Corporation. In December 1981 he became Professor of Measurement Technology and Instrumentation Science in the Department of Applied Physics, Technical University Delft, The Netherlands.

Dr. Young was a member of the Cytology Automation Committee of the National Cancer Institute from 1977 to 1981. He is currently on the Executive Council of the Society for Analytical Cytology and is an Associate Editor of its journal, *Cytometry*.

Balasubramanian, photograph and biography not available at the time of publication.

Douglas L. Dunbar, photograph and biography not available at the time of publication.

Ricardo L. Peverini received the B.S. degree in mathematics and biophysics from Pacific Union College, Angwin, CA, in 1978 and the M.S. degree in computing science from the University of California, Davis, in 1980.

He is currently pursuing the M.D. degree at Loma Linda University, Loma Linda, CA. From 1978 to 1980 he worked in the Biomedical Sciences Division of Lawrence Livermore National Laboratory, University of California, Livermore.

Mr. Peverini is a member of the Association for Computing Machinery.

Robert P. Bishop (S'76–M'80), photograph and biography not available at the time of publication.

An Ultrafast Laser Scanner Microscope for Digital Image Analysis

RICHARD L. SHOEMAKER, PETER H. BARTELS, DON W. HILLMAN, J. JONAS, DAVID KESSLER, ROLAND V. SHACK, AND DANIEL VUKOBRATOVICH

Abstract—**The design of an ultrafast laser scanner microscope has been completed and an experimental model has been constructed. The instrument is described and the considerations that led to our choice of scanning method and optical and electronic system design are discussed. The scanner incorporates numerous new technologic features, and promises to make high-resolution cell analysis practical at data rates comparable to those obtained now only in flow cytometry.**

INTRODUCTION

THE quantification of biologic processes by simple measurements either has been impossible until now because of their great complexity and diversity or has been restricted to very limited aspects of the biologic problem of interest. In the clinical diagnostic assessment of cells and tissues by pathologists, visual examination and long-term human experience, rather than a set of measurements, have been used to arrive at the diagnostic decision when subtle judgments were required. Only recently have technologic advances made it possible to apply measuring procedures of the required complexity to the evaluation of cell samples [1], [2]. These procedures can now provide diagnostic clues comparable to those attainable by human diagnosis and even exceed the capabilities of the human expert [3].

Quantitative cytology is a rapidly advancing field employing high technology. It follows two principal approaches to sample evaluation: 1) the technology of flow cytometry [4] and 2) digital image analysis at high resolution. Flow cytometry allows one to examine large samples of cells in suspension at very high speeds of typically several thousand cells/s. Cytochemical, physical, and immunologic markers characterize each cell and the properties of the cell population. The very high rates of throughput restrict the choice and the number of measures that can be collected. Digitized image analysis provides much more detailed information about each individual cell. However, digital image analysis and the computer processing of large numbers of cell images is not yet in use as a clinical diagnostic method because of the large information content of high-resolution imagery.

A survey of the technologic advances in the field of quantitative analytical cytology during the past decade shows that flow cytometry has flourished. Powerful analytical instrumentation is commercially available, and second- and third-generation models are in daily use both for research applications and

Manuscript received March 30, 1981; revised. This work was supported by the National Cancer Institute, Department of Health, Education and Welfare under Grant 1-R01-CA24466-01.

The authors are with the Optical Sciences Center, University of Arizona, Tucson, AZ 85721.

0018-9294/82/0200-0082$00.75